Accepted for publication in the Astronomical Journal
Preprint typeset using LaTeX style emulateapj v. 11/26/04

EVIDENCE FOR THE EVOLUTION OF YOUNG EARLY-TYPE GALAXIES IN THE GOODS/CDF-S FIELD

Thomas H. Puzia[1,2,3], Bahram Mobasher[3,4], and Paul Goudfrooij[3]

Accepted for publication in the Astronomical Journal

ABSTRACT

We have developed an efficient photometric technique for identifying young early-type galaxy candidates using a combination of photometric redshifts, spectral-type classification, and optical/near-infrared colors. Applying our technique to the GOODS HST/ACS and VLT/ISAAC data we have selected a complete and homogeneous sample of young elliptical candidates among early-type field galaxies. The distribution of structural parameters for these candidates shows that their selection, which is based on early spectral types, is fully consistent with early morphological types. We investigate the evolution of their luminosities and colors as a function of redshift and galaxy mass and find evidence for an increasing starburst mass fraction in these young early-type galaxy candidates at higher redshifts, which we interpret in terms of massive field galaxies experiencing more massive/intense starbursts at higher redshifts. Moreover, we find indications for a systematically larger young elliptical fraction among sub-$L^*/2$ early-type galaxies compared to their brighter counterparts. The total fraction among the field early-type galaxies increases with redshift, irrespective of galaxy luminosity. Our results are most consistent with galaxy formation scenarios in which stars in massive early-type field galaxies are assembled earlier than in their low-mass counterparts.

Subject headings: galaxies: K+A galaxies — galaxies: formation and evolution

1. INTRODUCTION

The last star-formation burst in galaxies defines their photometric appearance and is an important diagnostic of galaxy formation and evolution. The class of rejuvenated early-type galaxies includes so-called 'K+A' galaxies[5] which are objects that show spectroscopic signatures of old (K-type) and young (A-type) stellar populations (Dressler & Gunn 1983). The lack of emission lines in their spectra indicates that star-formation processes abruptly ceased ~ 1 Gyr ago, followed by a quiescent evolution into normal early-type galaxies (e.g. Couch & Sharples 1987).

Several scenarios have been suggested to explain this observed rejuvenation phenomenon: (1) galaxy-galaxy mergers (e.g. Zabludoff et al. 1996), (2) interactions of infalling galaxies with the intracluster medium (e.g. Gunn & Gott 1972; Bothun & Dressler 1986), (3) galaxy harassment (e.g. Moore et al. 1996, 1998), (4) tidally induced star formation (e.g. Byrd & Valtonen 1990), and (5) dusty starbursts (e.g. Poggianti et al. 1999; Poggianti & Wu 2000). While tidal interaction and galaxy harassment are important events in the overall context of galaxy formation and evolution (e.g, Bekki et al. 2005), they do not provide an obvious explanation for the sudden halt of star formation without invoking additional processes. Ram-pressure stripping and mergers are currently seen as the most viable scenarios to describe the ignition and sudden cessation of star formation in young early-type galaxies (e.g. Rose et al. 2001; Bekki & Couch 2003; Shioya et al. 2002, 2004; Quintero et al. 2004). Moreover, recent radio observations appear to exclude a dusty starburst scenario in general, as the measured radio fluxes are inconsistent with high star formation rates (i.e. $\gtrsim 10-100\ M_\odot\ a^{-1}$) for virtually all local post-starburst early-type galaxies (Miller & Owen 2001; Goto 2004). However, Smail et al. (1999) does find evidence for faint radio fluxes in spectroscopically confirmed post-starburst galaxies in distant dense clusters at $z \approx 0.4$.

K+A fractions are known to vary significantly with both redshift and environmental density. Several studies have revealed that the brightest K+A's in nearby clusters are sub-L^* systems (Caldwell et al. 1999; Poggianti et al. 2004), while at intermediate redshifts ($z \gtrsim 0.8$) K+As are found with $L \approx 3L^*$ (Dressler et al. 1999; Tran et al. 2003), suggesting an increase of K+A cluster galaxy mass with redshift. So far, the perhaps most unbiased comparison between the K+A fractions in field and cluster environments was done by Tran et al. (2003, 2004) who found a field K+A fraction of $\sim 3\%$ and a factor ~ 4 higher fraction in cluster environment for the redshift range $0.3 < z < 1$. Tran et al. further noted that the field K+A fraction shows strong fluctuations and is sensitive to selection criteria. Furthermore, the relatively short lifetime of the K+A signature ($\sim$1 Gyr, Couch & Sharples 1987; Belloni et al. 1995; Barger et al. 1996) implies that these galaxies are rare. This indicates the need for wide-area surveys to identify statistically significant samples of young early-type galaxies and determine their number fractions in both field and cluster environments. If their selection is performed consistently between datasets and galaxy formation models, their abundance may be a sensitive diagnostic for star-formation activity in field and cluster galaxies as a func-

[1] Herzberg Institute of Astrophysics, 5071 West Saanich Road, Victoria, BC, V9E 2E7, Canada
[2] Plaskett Fellow
[3] Space Telescope Science Institute, 3700 San Martin Drive, Baltimore, MD 21218
[4] Affiliated with the Space Sciences Department of the European Space Agency

[5] Historically, these galaxies were named "E+As" because of their early-type morphology appearance on the very first images. However, subsequent studies have shown that many of these galaxies contain significant disk components, so that the "E" becomes unjustified and is substituted by "K", owing to the spectral type of the underlying old stellar population (Franx 1993).

tion of redshift, making these rejuvenated objects useful tools to constrain hierarchical galaxy formation scenarios.

Keeping in mind that medium-resolution spectroscopy of all galaxies in large-area surveys is very expensive in terms of telescope time, the aim of this paper is to develop a photometric technique to identify young early-type galaxy *candidates* (hereafter yE candidates) for spectroscopic follow-up using a combination of photometric redshifts, spectral-type classification, and optical/near-infrared color-color diagrams. Applying this technique to the GOODS/CDF-S dataset (Giavalisco et al. 2004), we select a complete and homogeneous sample of yE candidates in the redshift range $0 < z \lesssim 1$. Finally, we investigate correlations between the colors of yE candidate galaxies with redshift and galaxy mass, which, if confirmed by spectroscopy, may put strong constraints on galaxy formation models. We use the standard ΛCDM cosmology parameters $\Omega_M = 0.3$, $\Omega_\Lambda = 0.7$, and $H_0 = 70$ km s^{-1} Mpc^{-1} throughout this work.

2. GOODS/CDF-S DATA

One of the two fields covered by the Great Observatories Origins Deep Survey (GOODS) Treasury Program is the *Chandra Deep Field South* (CDF-S) with optical HST/ACS and ground-based VLT/ISAAC near-infrared photometry (Giavalisco et al. 2004). These data span the wavelength range from near-UV to the near-infrared and provide ACS imaging with very high spatial resolution ($0.03''$) for ~ 86000 galaxies down to $V \approx 27.5$. Object detection and photometry was performed with SExtractor (Bertin & Arnouts 1996) after the images in all passbands were convolved to a common FWHM$\approx 0.45''$. The final magnitudes are the MAG_AUTO SExtractor magnitudes, which measure the total light.

Using the multi-waveband data available for galaxies in this field, photometric redshifts were measured following the technique presented in Mobasher et al. (2007). Briefly, this approach compares the template Spectral Energy Distributions (SEDs) for different spectral types of galaxies, shifted in redshift space, with the observed SED for galaxies detected in GOODS (see also Sect. 4.1). χ^2 fits are performed and the redshift and spectral type corresponding to the minimum χ^2 value are associated to those for the galaxy in question. The template spectral types consist of elliptical, Sbc, Scd, and Im-type galaxies from Coleman et al. (1980) and starburst templates from Kinney et al. (1996). Bayesian priors based on observed galaxy luminosity functions are used (as detailed in Mobasher et al. 2007). Comparison with galaxies with available spectroscopic redshifts yields a photometric redshift accuracy of $\sigma(\Delta z) = 0.03$ where $\Delta z = (z_{\rm phot} - z_{\rm spec})/(1 + z_{\rm spec})$.

In order to check the accuracy of our spectral types, we compare these with the morphology of galaxies measured from the GOODS-S ACS images. The morphologies are estimated using the concentration and asymmetry parameters (Conselice 1997; Abraham et al. 1996), measured for individual galaxies (B. Mobasher- private communication). We found a very good correlation between the morphology parameters and spectral types, particularly for elliptical galaxies. Therefore, we have reliable identification of elliptical galaxies, based on their spectral types, which constitutes the main selection criterion for the present study.

We use the information on redshifts and spectral types to compute K-corrections for all galaxies in our sample. Throughout the rest of this work we use AB magnitudes (Oke 1974)[6], and correct for Galactic foreground reddening $E_{B-V} = 0.008$ derived from the Schlegel et al. (1998) maps. We select galaxies brighter than $M_K = -19.0$ mag from the initial GOODS/CDF-S sample which have a mean photometric redshift accuracy of $\Delta z \leq 0.15$ corresponding to a 95% confidence interval. This photometric redshift uncertainty limit is introduced in order to keep the average color uncertainty below 0.15 mag due to k-corrections (see also Sect. 3). The final sample is volume-selected and complete to $z \approx 1$. We exclude objects where the photometry was compromised by saturated pixels, corrupted or truncated isophotal apertures, and where the extraction algorithm experienced problems during deblending or the photometric errors were larger than $\Delta m = 0.15$ mag in any filter. The final catalog includes objects with HST/ACS $BViz$ and VLT/ISAAC JHK_s magnitudes[7].

3. STELLAR POPULATION MODELS

3.1. *Diagnostic Colors*

Based on the Bruzual & Charlot (2003) simple stellar population (SSP) models and their 2003 version of the GALAXEV stellar population synthesis code, we compute optical/near-infrared photometric colors for composite stellar populations (CSP). We use the Salpeter IMF with limits at 0.1 and $100 M_\odot$. By comparison with the control sample of spectroscopically confirmed K+As, we identify the best diagnostic combination optical/near-infrared colors to select yE candidates.

Given the availability of many filters in our GOODS dataset ($BVizJHK_s$) we investigate several filter combinations that may most efficiently reduce the age-metallicity-extinction degeneracy in the color-color plane. Due to the presence of a hotter ~ 1 Gyr young stellar population, the B-band flux of yE galaxies is expected to be enhanced relative to older ($\gg 1$ Gyr) stellar populations. For slightly younger stellar populations with ages $\sim 0.4 - 0.8$ Gyr the Asymptotic Giant Branch (AGB) is densely populated with relatively cool stars (Renzini 1981) causing a stronger output in the near-infrared K-band (Persson et al. 1983). Since a small population of luminous thermally-pulsing AGB stars (TP-AGB) can significantly contribute to the integrated light of galaxies, the consideration of such short-lived evolutionary phases in SSP models is essential (Maraston 1998; Mouhcine & Lançon 2003). Past this so-called AGB-phase transition, near-infrared light is primarily sensitive to the mean temperature of the red giant branch, which is mainly driven by the luminosity-weighted mean metallicity of composite stellar populations.

In Figure 1 we show the effective filter throughputs for HST/ACS and the VLT/ISAAC instrument together with spectral energy distributions (SEDs) for single-burst stellar populations for ages $t = 290$ Myr, 640 Myr, 1.4 Gyr, 2.5 Gyr, and 11 Gyr at solar metallicity. For illus-

[6] AB magnitudes are defined by $m_{\rm AB} = -2.5 \log f_\nu - 48.6$, where f_ν is in ergs s^{-1} cm^{-2} Hz^{-1}. Alternatively, one can write $m_{\rm AB} = -2.5 \log f_\nu + 8.9$, where f_ν is the flux in Jy.

[7] In the following we shall refer to the K_s filter as the K band.

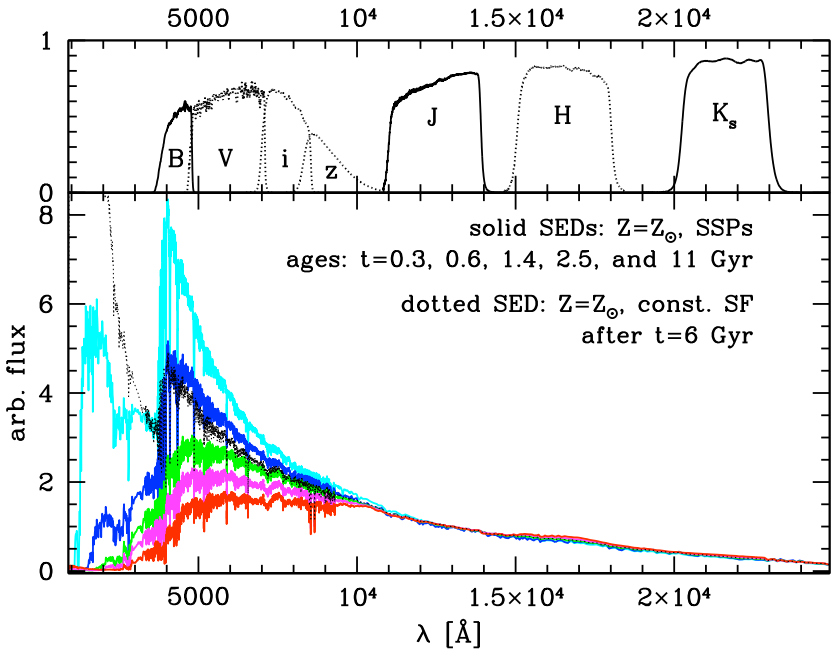

FIG. 1.— Comparison of restframe solar-metallicity SEDs for single-burst stellar populations with ages t = 290 Myr, 640 Myr, 1.4 Gyr, 2.5 Gyr, and 11 Gyr. A dotted line illustrates the SED of a solar-metallicity stellar population with a constant star formation rate after 6 Gyr. All SEDs were taken from Bruzual & Charlot (2003). Total filter throughputs for ACS and the ISAAC camera, including mirror reflectivity, window transmission, and detector quantum efficiency, are shown at the top of the panel.

tration purposes all SEDs were normalized to the flux at 1.3 μm. It is clear from the figure that the B band contains the most age-sensitive flux and that the $B-J$ color is a very good age indicator. It is instructive to note that the Lyman break is a sensitive indicator to identify constantly star-forming or very young post-starburst galaxies (i.e. $t \lesssim 0.5$ Gyr, see dotted SED in Fig. 1). However, the Balmer break is the more sensitive proxy to identify post-starburst galaxies with intermediate ages (i.e. $t \gtrsim 0.5$ Gyr), such as K+A galaxies. To find a good metallicity indicator we need to move to the near-infrared, past the z-band, where the continuum slope shows little impact of varying age. Here, the H-band continuum suffers from variations due to strong water vapor absorption, which is sensitive to the mean temperature of the stellar population (i.e. age-sensitivity). However, the relative continuum fluxes in J and K show little variation with age, and we define J–K as our best metallicity indicator which exhibits only modest age sensitivity during the AGB-phase transition (see also Ferraro et al. 2000).

The best choice of the most age-sensitive and the most metallicity-sensitive color depends also on data quality. For reference, the average color uncertainty introduced by the photometric redshift error is $\lesssim 0.15$ mag in both $B-J$ and $J-K$ for all galaxy types at $z \lesssim 1$. Given the mean uncertainty of all color combinations of our data, the most age-sensitive color is $B-J$ and the most metallicity-sensitive color is $J-K$, which is virtually independent of dust reddening. This BJK combination optimizes the selection of post-starburst intermediate-age stellar populations at redshifts $z \lesssim 1$. For higher redshifts, the age-metallicity degeneracy dilutes the age/metallicity sensitivity of this color combination as the restframe flux at $\lambda < 1$ μm moves into the J band, and a different filter combination is required.

A comparable photometric selection technique, although specifically targeting star-forming galaxies at higher redshifts, was described by Daddi et al. (2004). Similar techniques to detect intermediate-age globular clusters (i.e. single-burst stellar populations) in nearby galaxies have been recently used by Goudfrooij et al. (2001), Puzia et al. (2002), and Hempel & Kissler-Patig (2004).

3.2. *Spectroscopically confirmed K+As*

To test our photometric selection technique we use the K+A galaxy sample of Galaz (2000). This data set contains spectroscopically confirmed K+As in nearby ($z \approx 0.05$) and distant ($z \approx 0.3$) clusters and in the nearby field ($z \approx 0.1$). All galaxies have been classified as K+As (Couch & Sharples 1987; Franx 1993; Caldwell

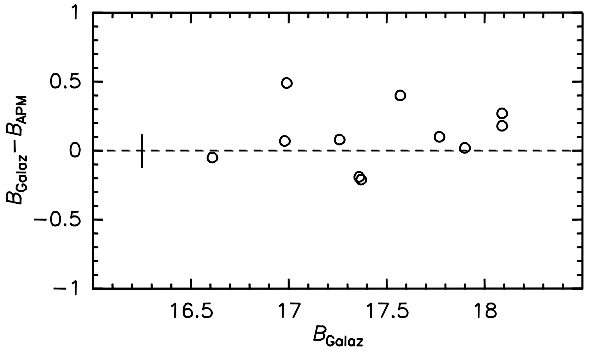

FIG. 2.— Comparison of B magnitudes for spectroscopically confirmed K+A galaxies taken from Galaz (2000) with those taken from the APM catalog. A vertical solid line shows the mean formal uncertainty.

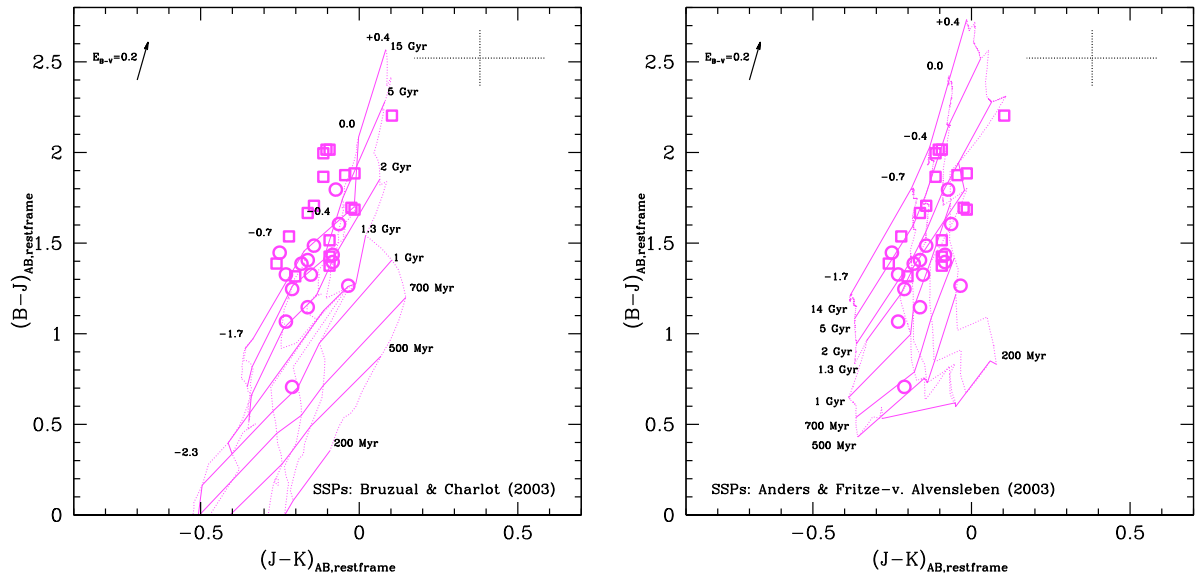

FIG. 3.— *Left panel*: Comparison of $(B-J)_{\rm AB}$ vs. $(J-K)_{\rm AB}$ restframe colors of spectroscopically confirmed K+A galaxies (*open symbols*) with SSP models of Bruzual & Charlot (2003). Open squares mark cluster K+A galaxies, open circles are field K+As. Isochrones (*solid lines*) are plotted for ages t = 200, 500, 700 Myr, and 1, 1.3, 2, 5, and 15 Gyr. Iso-metallicity lines (*dotted lines*) are shown for the metallicities [Z/H] $= -2.3, -1.7, -0.7, -0.4, 0.0$, and $+0.4$ dex. *Right panel*: Same data, but this time with SSP models of Anders & Fritze-v. Alvensleben (2003). Here isochrones (*solid lines*) were plotted for the ages t = 200, 500, and 700 Myr, and 1, 1.3, 2, 5, and 14 Gyr. Iso-metallicity tracks (*dotted lines*) are indicated for [Z/H] $= -1.7, -0.7, -0.4, 0.0$, and $+0.4$ dex. Each panel has the extinction vector for $E_{B-V} = 0.2$ mag indicated in the upper left corner. Mean uncertainties of the Galaz (2000) data are shown in the upper right corner.

& Rose 1997; Zabludoff et al. 1996), without any indications of emission lines. The near-infrared photometry of the Galaz study was performed with the Las Campanas NICMOS3 Hg:Cd:Te detector in the CIT filter system (Persson et al. 1998). We compute the transformations to the (Bessell & Brett 1988, hereafter BB) standard system using Bruzual & Charlot (2003) SEDs with ages from 0.2 Gyr to 15 Gyr and [Fe/H] values from −2.25 to +0.4 dex, and find the following (BB)–(CIT) transformations

$$J_{\rm BB} = J_{\rm CIT} - 0.0045 + 0.0102\,(J-K)_{\rm CIT}$$
$$(J-K)_{\rm BB} = 0.0147 + 0.9835\,(J-K)_{\rm CIT}$$

with RMS scatter of 0.0009 mag and 0.007 mag, respectively. Galaz' Table 2 lists Johnson B magnitudes as reported in NED[8] at the time, likely coming from various original sources. We compare these B magnitudes with those in the APM catalog[9] (Maddox et al. 1990) and show the comparison plot in Figure 2. We find significant offsets for the optical photometry between the Galaz and the APM catalog. Since the magnitudes in the APM catalog were derived in an internally consistent way, we adopt the APM B magnitudes for further analysis in this paper. The mean uncertainties in BJK colors of the comparison sample are 0.12, 0.10, and 0.18 mag, respectively. All optical and near-infrared magnitudes from the GOODS catalog and the comparison sample represent total magnitudes.

3.3. *Confirmed K+As in the BJK color-color plane*

In Figure 3 we compare $(B-J)_{\rm AB}$ vs. $(J-K)_{\rm AB}$ restframe colors of spectroscopically confirmed K+A galaxies with SSP model predictions from two different groups: Bruzual & Charlot (2003, hereafter BC03) and Anders & Fritze-v. Alvensleben (2003, hereafter AF03). The BC03 predictions were calculated in the AB system with the same filter transmission functions as the GOODS/CDF-S data. For the AF03 models, which are tabulated in Vega-based magnitudes using the BB filter system, we follow the Vega-AB transformations: $K_{\rm AB} = 1.891 + K_{\rm Vega}$, $J_{\rm AB} = 0.91 + J_{\rm Vega}$, and $B_{\rm AB} = -0.105 + B_{\rm Vega}$. As expected, the location of confirmed K+As in the color-color plane corresponds to old to intermediate ages. We find that the absolute age calibration differs between the two models. The BC03 models predict (luminosity-weighted) ages between ∼15 and ∼2 Gyr for most K+As, while the models of AF03 predict younger ages in the range ∼1−5 Gyr. The metallicity scales on the other hand are very similar in both models. The majority of confirmed K+A galaxies have luminosity-weighted metallicities between [Z/H] ≈ −0.7 and 0.0 dex, with few outliers at super-solar metallicities, which might be reddened objects.

3.4. *Composite Stellar Populations in the BJK Color-Color Plane*

Several groups compared the mean colors of K+A galaxies using optical and near-infrared photometry with population synthesis models (e.g. Newberry et al. 1990; Belloni et al. 1995; Barger et al. 1996; Shioya et al. 2002; Balogh et al. 2005). In this work we combine spectral-type fitting with model predictions and investigate the influence of different metallicities and mass fractions of the starburst population on colors and luminosities of post-starburst galaxies in the optical/near-infrared color-color plane and in color-magnitude diagrams.

Figure 4 shows the evolution of BC03 isochrones where a starburst is ignited after 10 Gyr of passive SSP evolution. Assuming a minor merger, we assign 10% of the

[8] the NASA/IPAC Extragalactic Database, http://nedwww.ipac.caltech.edu

[9] http://www.ast.cam.ac.uk/~apmcat

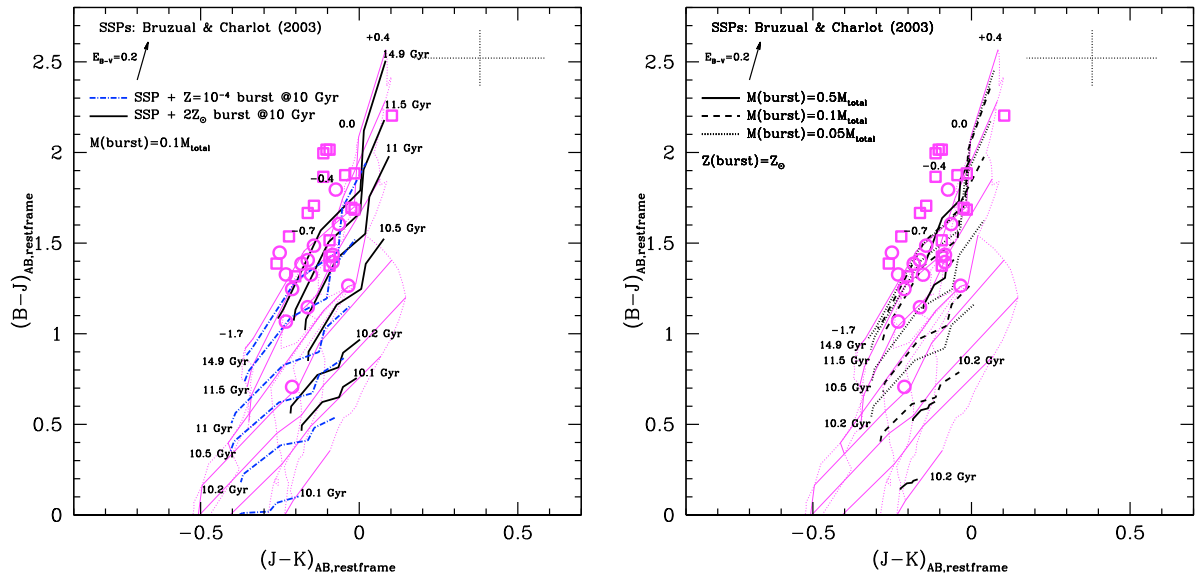

FIG. 4.— *Left panel*: Evolution of $(B-J)_{\rm AB}$ vs. $(J-K)_{\rm AB}$ restframe colors for an SSP with a starburst that ignites after 10 Gyr of passive evolution and decays for another 5 Gyr. Two set of isochrones with ages $t = 10.1, 10.2, 10.5, 11, 11.5$, and 14.9 Gyr are shown for the metallicities [Z/H] = 0.4 (*solid lines*) and −2.3 dex (*dot-dashed lines*) of the starburst stellar population. The starburst strength amounts to 10% of the total final stellar mass. *Right panel*: Evolution of colors for different starburst strengths/masses for a solar metallicity burst. Ischrones for ages $t = 10.2, 10.5, 11.5$, and 14.9 Gyr are plotted with different line types (*solid, dashed,* and *dotted lines*) indicating the dependence on starburst mass $M_{\rm burst} = 0.05, 0.1$, and 0.5 $M_{\rm total}$. For reference we overplotted in both panels the SSP model grid from the left panel of Figure 3. All predictions were computed using the SSP models of Bruzual & Charlot (2003). Spectroscopically confirmed K+A galaxies are as in Figure 3.

final stellar mass to the starburst population. We adopt two metallicities Z = 0.04 (twice solar metallicity) and Z = 10^{-4} ([Z/H] = −2.3 dex) for the starburst stellar population, which are superposed on top of the full range of metallicities ([Z/H] = −2.3 to +0.4 dex.) of the underlying, older stellar population. Note the significant difference in $B-J$ colors during the first ∼1.5 Gyr after the starburst. If determined relative to passively evolving galaxies, this color offset is a sensitive post-starburst indicator and will be discussed below in more detail.

In the right panel of Figure 4 we show the influence of changing starburst mass fraction on the post-starburst galaxy colors. This time we choose solar metallicity for the starburst with mass fractions are 5%, 10% (minor merger), and 50% (major merger) of the final total stellar mass. The Figure illustrates that the higher the starburst mass fraction the bluer the $B-J$ color is during the post-starburst phase, in agreement with previous studies (e.g. Barger et al. 1996). In addition, there is a mass fraction-metallicity degeneracy of post-starburst near-infrared colors. Metal-rich major starbursts can exhibit the same $J-K$ colors as metal-poor minor starbursts. This degeneracy is most prominent for intermediate metallicities in the range $-0.7 \lesssim$ [Z/H] $\lesssim 0$. For more extreme metallicities the burst strength can be constrained with increasing confidence. In other words, yE galaxies with starburst mass fractions $\lesssim$ 10% and $J-K \gtrsim 0$ are likely to have experienced a recent starburst with super-solar metallicity. The same mass-fraction limit and $J-K \lesssim -0.3$ mag indicate sub-solar starburst metallicities.

In summary, B–J is mainly degenerate in age and starburst mass fraction, $J-K$ is mainly degenerate in metallicity and starburst mass fraction. We conclude that the $B-J$ vs. $J-K$ color-color plane can be used to identify post-starburst galaxies. But only extreme metallicities of the post-starburst stellar population can be narrowed down robustly. The color-color plane is not suitable to derive starburst mass fractions for intermediate metallicities without any other information. However, these degeneracies can be partly lifted by including restframe K-band luminosities. Our findings are relatively independent of the choice of SSP models, as the systematics in the AF03 models give the same results.

4. SELECTION OF YE CANDIDATES

4.1. *Spectral Types*

In the following we develop a robust method to identify yE galaxy candidates from the GOODS/CDF-S photometric catalog using a combination of photometric redshifts, spectral-type classification, and optical/near-infrared colors. The photometric redshifts and spectral types are measured by using template SEDs, shifting them in redshift steps and performing χ^2 fits to the observed SEDs at each step. The templates corresponding to the minimum χ^2 values are selected, with its spectral type and redshift assigned to the galaxy in question. We use the observed templates for elliptical, Sbc, Scd and Im-type galaxies from Coleman et al. (1980) and the starburst SEDs from Kinney et al. (1996). In order to increase the resolution in spectral types, we also divide the interval between adjacent spectral classes into two intermediate bins. For instance, between the two discrete spectral types for ellipticals ($T = 1$) and Sbc-type spectra ($T = 2$) we include two discrete sub-categories ($T = 1\frac{1}{3}, 1\frac{2}{3}$) that are linear mixtures between the two boundary types. This allows a more continuous spectral classification across the Hubble types while not causing degeneracy. The choice of steps of 1/3 unit was made as a

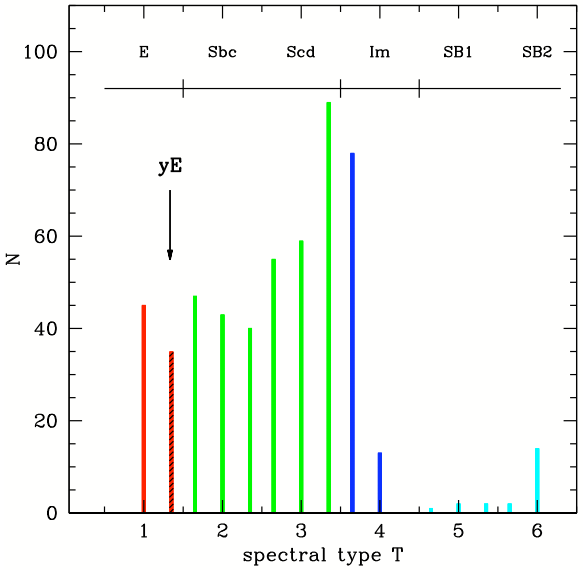

FIG. 5.— Distribution of spectral types T that were assigned by the photometric redshift routine for all objects in our selected GOODS/CDF-S sample (for details on the photometric redshift fitting routine we refer the reader to Mobasher et al. 2004, 2007). The locations of individual spectral types are labeled. A sub-population of several objects have a slightly earlier spectral type ($T=1\frac{1}{3}$) than passively evolving galaxies ($T=1$). These are our yE candidates and are marked in the plot with a hatched bin.

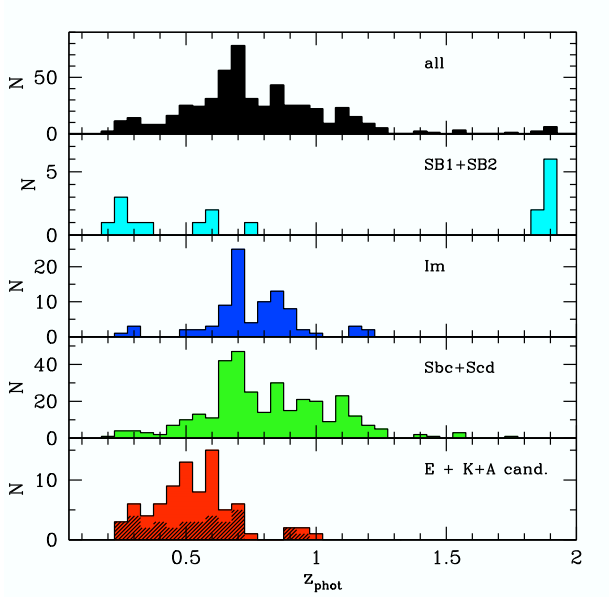

FIG. 6.— Distribution of photometric redshifts for all selected objects in our GOODS/CDF-S photometric dataset (for details on the photometric redshift routine see Mobasher et al. 2004). The parametrization by spectral-type is identical to the one in Figure 5.

compromise between the goal to increase the resolution of spectral types on one side and the goal to avoid creating degeneracies in the phot-z routine on the other. Details of the photometric redshift and spectral-type measurement are presented in Mobasher et al. (2004, 2007). We plot the distribution of the discrete spectral types in Figure 5 and define all objects that were assigned slightly earlier spectral types ($T=1\frac{1}{3}$) than passively evolving galaxies ($T=1$) as yE candidates, i.e. objects which are bluer than normal ellipticals but redder than normal early-type spirals. Their location in Figure 5 is marked by a hatched histogram. Because later galaxy types can exhibit similar BJK colors as genuine yE galaxies, we use the spectral-type information to exclude late-type star-forming galaxies and to include only galaxy candidates with early spectral types in the following analysis. The distribution of photometric redshifts of all objects is shown in Figure 6. Most of our yE candidates have redshifts between $z\approx 0.2$ and 0.8, with few objects at slightly higher redshifts $z\approx 1.0$.

4.2. *Morphologies*

To investigate the yE candidate morphologies we cross-correlate the GOODS/CDF-S sample with the structural parameter classification of Ravindranath et al. (2006). Based on the $BViz$ HST/ACS images the authors computed CAS parameters ('asymmetry', 'concentration', and 'smoothness' defined in Conselice 2003) for all our sample sources. Because of the redshift distribution of our sources each ACS filter probes a different wavelength and therefore a different morphological (stellar) component in a galaxy. To allow a comparison of structural parameters that is independent of redshift we compute the redshift-corrected restframe B-band morphologies by linearly interpolating the CAS parameters between the pivot wavelengths of each ACS filter (see Sirianni et al. 2005) according to the redshift of each source. In Figure 7 we show the distribution of rest-frame B-band CAS parameters for all sample galaxies sub-divided by spectral-type as in Figure 5. We find that the overall spectral-type classification of our yE candidates is consistent with early-type morphologies, which confirms the robustness of our procedure to select early-type post-starburst galaxies. In particular, the distribution of the CAS 'concentration' parameter indicates that very few yE candidate galaxies with later-type morphologies were selected by our photometric selection.

4.3. *BJK Color-Color Diagram*

The left panel of Figure 8 shows the GOODS/CDF-S data in the BJK color-color plane. Different symbols depict different spectral types as assigned to each object by the photometric redshift fitting routine. Most objects with SEDs consistent with passive early-type galaxies clump around restframe $(B-J)_{\rm AB}\approx 1.9$ and $(J-K)_{\rm AB}\approx 0$. Objects with slightly later SED types (our yE candidates) scatter towards bluer B–J colors and have intermediate J–K colors that place their mean locus between spiral and star-forming galaxies. *We find that the spectral-type selection is consistent with the BJK color selection and morphological classification.* Moreover, most yE candidates are consistent with the previously computed composite stellar population models for post-starburst galaxies. Only one yE candidate at $(B-J)_{\rm AB}\approx 1.6$ and $(J-K)_{\rm AB}\approx 0.35$ deviates significantly from the model predictions and might be a dusty starburst. For reference, we plot the control sample of spectroscopically confirmed K+As (open symbols).

To provide a comparison independent of SSP model predictions we show in the right panel of Figure 8 nearby early-type (taken from Michard 2005) and late-type galaxies (taken from Pérez-González et al. 2003a) in the same color-color plane as the GOODS/CDF-S

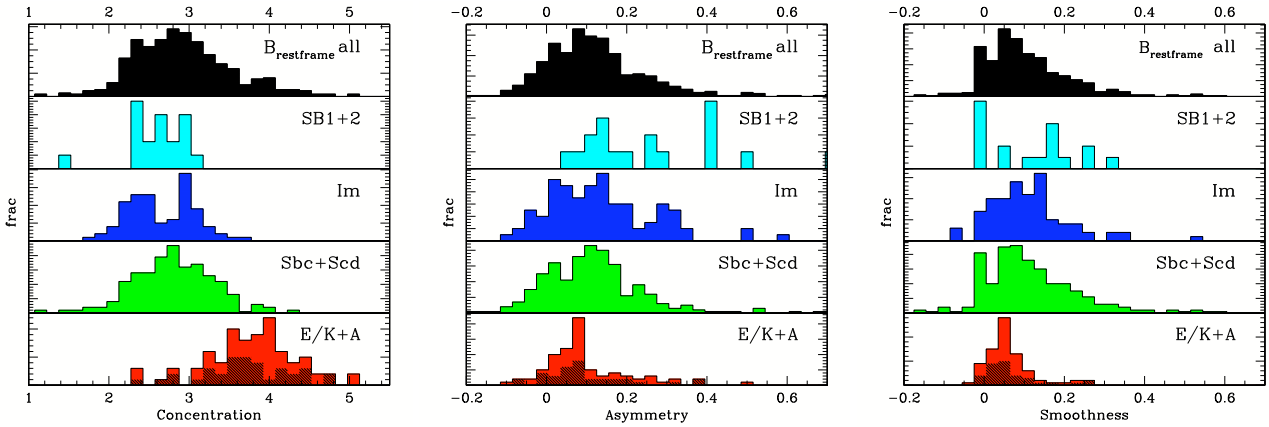

FIG. 7.— Distribution of restframe B-band CAS parameters (concentration, asymmetry, and smoothness, see Conselice 2003) taken from Ravindranath et al. (2006) for all selected objects in our GOODS/CDF-S photometric dataset parameterized by their spectral type as in Figure 5. Note the strong separation of yE candidates in the concentration parameter (*left panel*) from galaxies with later spectral types.

TABLE 1
COMPARISON BETWEEN PHOTOMETRIC AND SPECTROSCOPIC REDSHIFTS.

subsample	$\langle\Delta z\rangle^{a}$	σ	N
E	-0.109 ± 0.004	0.061	14
yE	-0.119 ± 0.012	0.083	7
Sab	0.028 ± 0.004	0.134	37
Scd	-0.061 ± 0.046	0.185	4
Starburst	0.224 ± 0.000	...	1

[a] $\langle\Delta z\rangle = \langle z_{\rm phot} - z_{\rm spec}\rangle$.

data. We find a good agreement between the early-type galaxies in GOODS/CDF-S and the local galaxy sample. However, the smaller photometric errors of the local galaxy sample allow a more clearly detected offset of the spectroscopically confirmed K+A galaxies towards bluer $B-J$ colors (i.e., younger ages) compared to the local early-type galaxies, which line up in a tight sequence. We also notice that fewer spiral (squares) and Irr galaxies (triangles) lie outside of the SSP grid which is likely again, partly due to smaller photometric errors of the nearby sample. We investigate whether this disagreement may be due to systematics in the photometric redshift determination, but find no differences in the error distributions between spiral and irregular galaxies, in particular in $J-K$ that appears to be primarily responsible for the scatter. A matching between the photometric redshifts of our sample and currently available spectroscopic redshifts from the literature (Le Fèvre et al. 2004) results in good agreement (see Table 1). Although we compare restframe colors in both samples, the galaxies in our GOODS/CDF-S data are more distant than the nearby comparison sample. Evolutionary factors, such as possibly enhanced dust fractions, may be responsible for the enhanced scatter in our data. Deep mid-IR imaging and optical to infrared spectroscopy should be able to resolve this issue.

We define the population of yE galaxy candidates as those objects that have slightly later spectral types ($T = 1\frac{1}{3}$, see Fig. 5) and BJK colors that are inconsistent with passively evolving (reddest) early-type galaxies. The selected yE candidates are marked in Figure 8 by red circles with central black dots. This definition might exclude some genuine K+As since the control sample contains some spectroscopically confirmed K+A galaxies (in galaxy clusters) with BJK colors consistent with passively evolving early-type galaxies. Taking into account the average photometric error, this fraction is expected to be less than $\sim 15\%$. We point out that even with the color, spectral-type, and morphology selection, our yE candidate sample may be contaminated by early-type spiral galaxies that can mimic the morphologies of elliptical galaxies (e.g., when in a largely face-on configuration) and the SEDs of yE candidates because of their low, but continuous star formation rates. Based on the local comparison sample we estimate this contamination fraction between $\sim 10-30\%$, depending on the exact color selection. Again, deep follow-up spectroscopy should be able to address this contamination fraction.

5. DISCUSSION

5.1. *Color-Magnitude Diagrams*

Post-starburst galaxies tend to be brighter in the optical than their passive counterparts (e.g. Tran et al. 2003), which is likely due to their additional ~ 1 Gyr old stellar population. However, optical photometry is not able to provide strong constraints on how the stellar masses of these rejuvenated galaxies compare with those of passively evolving galaxies. The K-band stellar mass-to-light ratio changes by a factor of ~ 3 from ~ 1.5 Gyr to 13 Gyr (see also Drory et al. 2004), which is about an order of magnitude smaller a change than in the optical. M/L_K changes by about a factor 1.5 between 500 Myr and 1.5 Gyr (the K+A phase). Hence, relative to optical colors a M_K selection defines the best approximation to a stellar-mass selected dataset.

In Figure 9 we show color-magnitude (CM) diagrams for all early-type galaxies ($T \leq 1.5$) and the selected yE candidates as well as the K+A control sample and nearby ellipticals. Overplotted are color-magnitude relations for early-type galaxies taken from the large galaxy survey of Mobasher et al. (1986), in good agreement with the GOODS data and the nearby elliptical galaxy sample. We find no significant difference between red-sequence galaxies and yE candidates in the near-infrared $J-K$ vs. M_K diagram, but we detect a significant offset in the $B-J$ vs. M_K diagram where the yE candidates

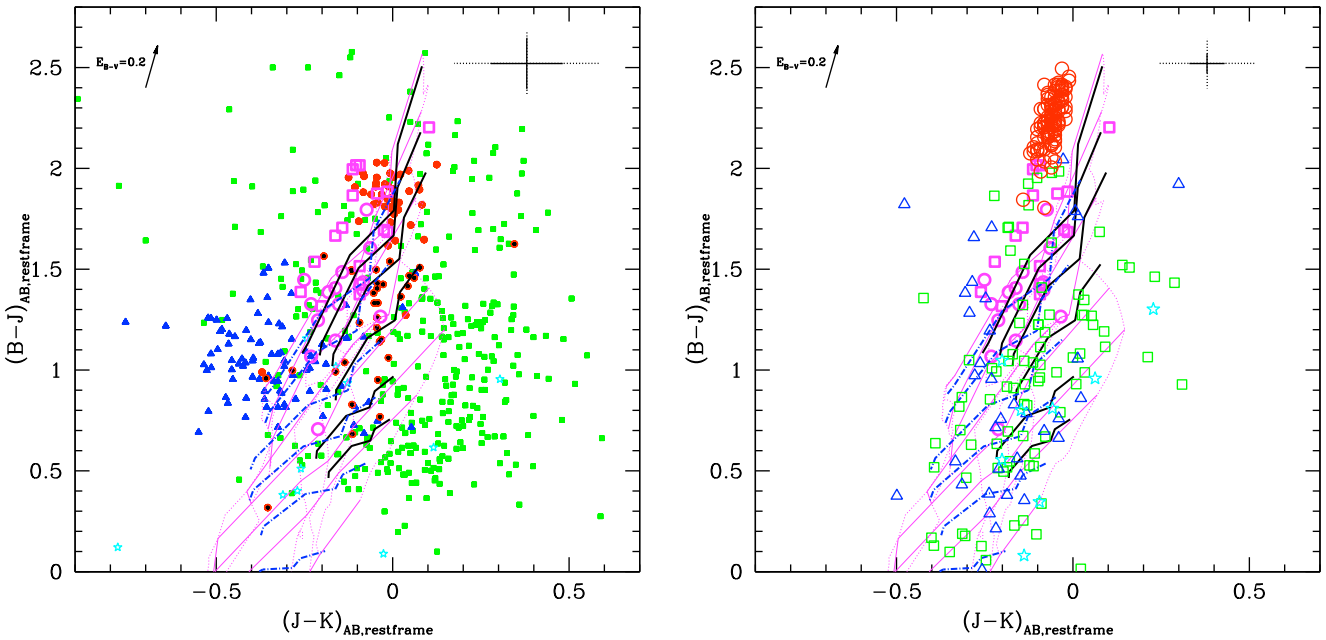

FIG. 8.— *Left panel*: BJK color-color diagram (using de-reddened rest-frame AB magnitudes) of galaxies in the GOODS/CDF-S Field. The data symbols are parameterized by the galaxy spectral types, and are early-type (*filled circles*), spiral (*filled squares*), irregular (*filled triangles*), and starbursts (*stars*). yE galaxy candidates are marked by *small dark dots*. Spectroscopically confirmed K+A galaxies taken from Galaz (2000) are indicated by open symbols, where open squares mark cluster K+A galaxies and open circles are field K+As. Average total photometric errors, including uncertainties of the photometry and the photometric redshift determination, are indicated in the upper right corner for yE candidates (*solid cross*) and the mean photometric uncertainties for confirmed K+A galaxies (*dotted cross*). *Right panel*: BJK color-color diagram for local galaxies. Open circles are nearby ellipticals from Michard (2005), open squares and triangles are Sab and Scd spirals, while stars show local starburst galaxies, both taken from Pérez-González et al. (2003a). The same spectroscopically confirmed K+A sample as in the left panel is overplotted for comparison. The solid error bar shows average uncertainties for the elliptical sample, while the dotted cross is for the later-type galaxies. SSP models in both panels are identical to those in the left panel of Figure 4.

have significantly bluer colors at the same M_K (stellar mass) compared to the red sequence.

We show the influence of changing luminosity-weighted age (Δt), metallicity (ΔZ), total galaxy mass ($\Delta M_{\rm gal.}$), and starburst-mass fraction (ΔM_*) as vectors in both CM diagrams. Δt and $\Delta M_{\rm gal.}$, and ΔZ and ΔM_* are highly degenerate in the $J-K$ vs. M_K diagram. In fact, the Δt and $\Delta M_{\rm gal.}$ vectors are almost parallel to the red sequence (see upper panel in Fig. 9) and have, therefore, negligible influence on the scatter in the $J-K$ color, which is mainly driven by metallicity and the starburst-mass fraction. The relatively small scatter in this diagram hints at a small scatter in metallicity and starburst-mass fraction and/or is a signature of a correlation between these parameters. This degeneracy can be partly lifted with the $B-J$ vs. M_K diagram (see below). Four yE candidates fall significantly off the red sequence in the $J-K$ vs. M_K diagram. They are likely to have experienced significantly different starburst events than the rest of the sample. One possible explanation is that the metallicity of their starburst population is significantly lower.

The most influential parameters in the $B-J$ vs. M_K diagram are age and the starburst mass fraction (besides the total galaxy mass). Both vectors are highly inclined relative to the red sequence, which is a graphic explanation of the scatter in this plot. Metallicity plays a negligible role. We use the $B-J$ vs. M_K diagram to discuss the redshift evolution of our yE candidates in the next section.

5.2. *Starburst Mass Evolution*

In the hierarchical merging scenario of galaxy formation, massive structures are expected to form on extended timescales from smaller sub-units with a considerable fraction of stars forming relatively recently (e.g. Springel et al. 2005). If, in contrast, more massive structures form first, as seen in the monolithic collapse scenario, the majority of stars form at high redshifts ($z \gtrsim 2$) in intense starbursts (e.g. Larson 1975). The fraction of yE signatures among massive early-type galaxies is a measure of dissipative merging activity (recently often named "wet merging"), which is expected to be a function of redshift in the hierarchical merging picture. In contrast, no such evolution is expected in the early monolithic collapse scenario out to $z \sim 2$. This difference is expected to depend on environment and to be more pronounced in the field (Benson et al. 2002), which we probe here with the GOODS dataset. The fraction of yE galaxies and the strength of the yE signatures among massive early-type field galaxies as a function of redshift therefore puts strong constraints on galaxy formation models.

To investigate the redshift evolution of our yE candidates, we subdivide the sample into four redshift bins between $z = 0$ and 1. For each galaxy we determine the $B-J$ offset with respect to the red sequence and plot the residuals versus their absolute K-band luminosity in Figure 10. Our analysis is limited in redshift space by the completeness of our GOODS data in the K band. A 10σ point source detection in the VLT/ISAAC data is feasible down to m_K(AB) = 25.1 mag (Giavalisco et al. 2004),

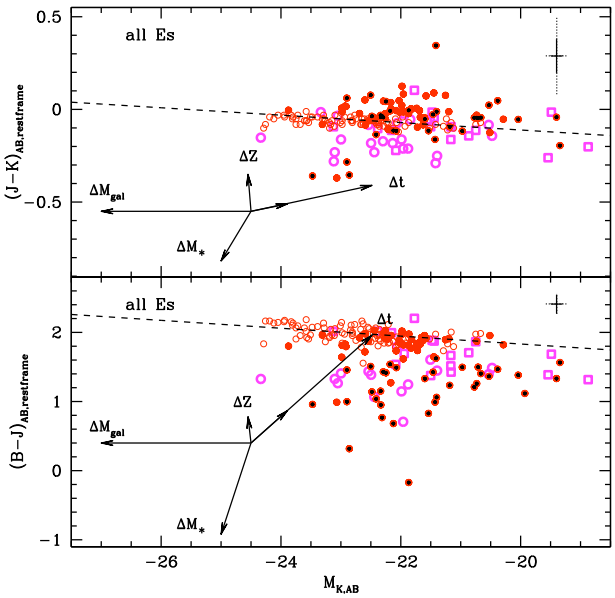

FIG. 9.— Optical/near-infrared color-magnitude diagrams of early-type galaxies (*filled circles*) and yE candidates (*dotted circles*). Large open (magenta) symbols mark spectroscopically confirmed K+As (Galaz 2000) in the field (*circles*) and cluster environment (*squares*). Small open (red) circles are nearby elliptical galaxies from Michard (2005), as in the right panel of Figure 8. The nearby data were corrected for passive evolution, according to Bruzual & Charlot (2003) models, to the reference redshift $z = 0.5$ of our GOODS data, which includes only a correction of $\Delta(B-J) = 0.2$ mag. Arrows indicate the relative changes in Δt between 500 Myr and 1.5 Gyr (short arrow), and 500 Myr and 13 Gyr (long arrow), ΔZ between $0.2Z$ and solar metallicity, $\Delta M_{\rm gal.}$ between 10^{10} and $10^{11} M_\odot$, and ΔM_* between 5% and 50% of the starburst mass fraction. Color-magnitude relations for early-type galaxies from the survey of Mobasher et al. (1986) are overplotted as dashed lines. Average photometric errors of yE candidates (*solid cross*) and spectroscopically confirmed K+As (*dotted cross*) are plotted in the upper right corner of each panel.

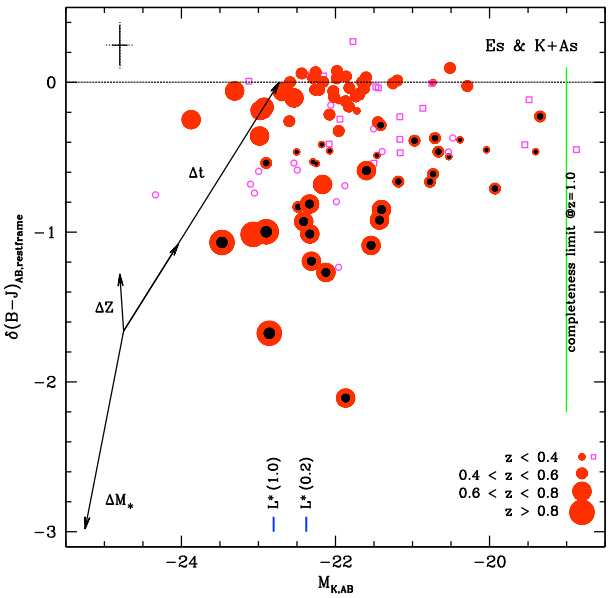

FIG. 10.— Residual $B-J$ colors with respect to the red sequence (see Fig. 9) as a function of absolute K band magnitude for early-type galaxies. Dark dots mark yE candidates. Open symbols indicate spectroscopically confirmed K+A as in Fig. 9; taken from Galaz (2000). The symbols size is parametrized by redshift. All confirmed K+A galaxies are located at redshifts $z \leq 0.12$. Vectors indicate the influence of varying age, metallicity, and starburst mass fraction as in Fig. 9. Average photometric errors are indicated in the upper left corner of the panel, where the dotted cross indicates typical errors of the confirmed K+As and the solid cross shows errors for yE candidates. A long vertical line shows the 10σ points source detection limit at $z = 1$. Small vertical lines indicate L^* at redshifts 0.2 and 1.0 for field galaxies (Drory et al. 2003). Note the paucity of yE candidates at magnitudes fainter than $M_{K,\rm AB} \approx -21.2$ and $\delta(B-J)_{\rm AB} \lesssim -0.8$ mag.

which translates into $M_{K,\rm AB} = -19.0$ mag at a redshift of $z = 1$ (indicated by a vertical line in Figure 10). Hence, completeness is not an issue for the following analysis.

We observe that at any given M_K the B–J residuals are systematically larger for higher redshift galaxies. Spectroscopically confirmed K+As show a similar trend, but their redshift range is significantly smaller ($z \leq 0.12$) than that of our sample ($z \leq 1$, see Fig. 6). Note that confirmed field K+As show larger $\delta(B$–$J)$ than confirmed cluster K+As, which lie closer to the red sequence. We also find tentative evidence for a systematic difference in $\langle\delta(J-K)\rangle$ between confirmed *field* K+As (open circles) and the combination of our yE candidates and confirmed *cluster* K+As. It appears that a metallicity difference is the most obvious way to explain this offset, given that in the more age-sensitive $B-J$ panel the yE candidates lie among, or are bluer than, the nearby confirmed field and cluster K+As. However, the photometric errors of the spectroscopically confirmed K+A sample require that this intriguing result be confirmed with deep spectroscopy.

Parameters likely responsible for the evolution in $\delta(B$–$J)$ with redshift are *(i)* a younger age of the post-starburst population at higher redshift, or *(ii)* a larger mass fraction of the post-starburst population at higher redshifts (we established in Section 3 that metallicity has a smaller effect on $\delta(B-J)$). First we consider age effects. Under the assumption that the yE candidates indeed host $0.5-1.5$ Gyr old post-starburst populations with strong Balmer absorption-line spectra, the vectors in Figure 10 show that the difference in $\delta(B$–$J)$ between yE candidates with $z \lesssim 0.4$ and those with $z > 0.6$ is in principle similar to the effect of age fading from 0.5 to 1.5 Gyr. However, it is hard to imagine that post-starburst populations in yE galaxies at higher redshift (be it induced by galaxy interactions or by ram-pressure stripping) would be systematically younger than in low-redshift ones, given the short duration of the yE phenomenon relative to the difference in look-back times within this redshift range. In the adopted WMAP cosmology, the difference in look-back times between $z = 0.2$ and 1.0 is $7.8 - 2.4 = 5.4$ Gyr, significantly longer than the duration of the yE phenomenon. Instead, one would expect the ages of such post-starburst populations to be randomly distributed (between 0.5 and 1.5 Gyr) at any redshift. We, therefore, suggest that it is more likely that the increase of yE candidates' $\delta(B-J)$ with redshift is primarily due to an *increasing mass fraction of the post-starburst population*. If indeed the yE phenomenon identifies an important era in the assembly history of early-type galaxies, the lack of low-luminosity ($M_K \gtrsim -21$) yE candidates at $z > 0.6$ in our GOODS sample would constitute strong evidence in favor of galaxy formation

scenarios in which more massive early-type galaxies in the field are assembled earlier than their low-mass counterparts, which is in line with the "downsizing" picture (e.g. Cowie et al. 1996).

On the other hand, we currently cannot exclude the possibility that the higher-redshift yE candidates do not actually host a (one) post-starburst population, but instead have systematically younger overall (luminosity-weighted) ages than the lower-redshift yE candidates. More frequent bursts at higher redshifts, due to more frequent mergers, might be a possible explanation, which would lead to systematically younger observed ages. Given the relevance of this issue in terms of its power to constrain early-type galaxy formation scenarios, we suggest a spectroscopic followup to test whether our yE candidates really do contain K+A features in their spectra.

5.3. *Evolution of the yE Fraction*

The fraction of post-starburst galaxies in nearby clusters was reported to increase with decreasing galaxy luminosity (e.g. Poggianti et al. 2001; Smail et al. 2001). The morphology bias prevents a direct comparison between the yE fractions in the cluster and field environment. We, therefore, select only early-type galaxies from our sample and investigate the yE fraction in the field. A similar trend of an increasing post-starburst fraction with decreasing galaxy luminosity is present in our GOODS sample of field galaxies. We quantify this trend by splitting the data at $L^*/2$ along the pure luminosity evolution vector and counting the number of passive Es and yE candidates. The corresponding values for the division for each redshift bin into super-$L^*/2$ and sub-$L^*/2$ systems are $M_K^* = -22.27, -22.43, -22.64$, and -22.75 mag for $z = 0.3, 0.5, 0.7$, and 0.9, respectively. Note that the samples are complete down to $M_B = -16.3$ mag and $M_K = -19.0$ mag at $z=1$, which leaves our sample sensitive to objects with restframe colors $B-K \lesssim 2.7$ mag, but excludes extremely reddened objects, such as EROs (e.g. Daddi et al. 2000). However, these galaxies are most frequent beyond redshift unity (e.g. Georgakakis et al. 2006; Simpson et al. 2006) and are expected not to be a significant part of our initial sample. To improve sample statistics we merge the number counts of the two upper and two lower redshift bins, which results in a high and low-redshift sample divided at $z = 0.6$. Galaxy number counts are given in Table 2.

We confirm the trend of a higher fraction of post-starbursts among early-type galaxies toward less luminous objects. In the high-redshift sample we find a yE candidate fraction of 86% among all sub-$L^*/2$ early-type galaxies, whereas only 22% of the more luminous (massive) objects are yE candidates. The yE fractions shrink towards lower redshifts to 51% for sub-$L^*/2$ systems and 11% for their brighter counterparts. We suggest that these high yE fractions be confirmed (or refuted) using follow-up spectroscopy.

TABLE 2
Number counts of E galaxies and yE candidates.

	sub-$L^*/2$		$> L^*/2$			
redshift	$N_{\rm E}$	$N_{\rm yE}$	$N_{\rm E}$	$N_{\rm yE}$	$f_{<L^*/2}$[a]	$f_{>L^*/2}$[b]
$z > 0.6$	2	12	7	2	0.86	0.22
$z < 0.6$	18	19	16	2	0.51	0.11

[a]Fraction $f_{<L^*/2}$ of yE galaxy candidates among all sub-$L^*/2$ early-type galaxies.
[b]Fraction $f_{>L^*/2}$ of yE galaxy candidates among all $> L^*/2$ early-type galaxies.

6. CONCLUSIONS

Based on the combination of photometric redshifts, spectral-type classification, and optical/near-infrared colors, we have selected a sample of young early-type galaxy candidates (yE candidates) from the GOODS/CDF-S dataset. Our technique relies on spectral-type fitting and color-color/color-magnitude diagnostic diagrams and provides an efficient method for selecting yE candidates using *only* photometric information. An analysis of CAS parameters shows that the selected yE candidates have early morphological types, which confirms that spectral-type and morphological-type selection are fully consistent with each other. The comparison of population synthesis models and observed properties of a sample of spectroscopically confirmed K+A galaxies provides strong circumstantial evidence that the selected candidates are genuine field early-type post-starburst galaxies.

We study the systematics that drive colors and magnitudes of post-starburst galaxies in diagnostic diagrams using current population synthesis models. Our analysis reveals evidence for a changing starburst mass fraction with increasing redshift in the sense that more massive/intense starbursts may be responsible for the yE signatures of massive field early-type galaxies at higher redshifts. Furthermore, we find a higher yE candidate fraction in sub-$L^*/2$ early-type galaxies compared to their more luminous counterparts. Within the redshift range of our data ($z \lesssim 1$) we may be witnessing evidence for enhanced merging in the field towards higher redshifts, especially for high-luminosity galaxies. Similar results are obtained by studies of luminosity-weighted mean ages of nearby early-type galaxies which indicate that low-L galaxies show a much greater scatter to younger luminosity-weighted mean ages than high-L galaxies (e.g. Caldwell et al. 2003; Pérez-González et al. 2003b; Sánchez-Blázquez et al. 2006). If follow-up spectroscopy of the yE candidates identified in this paper confirms their K+A nature, this suggests that the assembly of stars in high-L early-type field galaxies occurred earlier than in their lower-L counterparts.

We thank Peter M. Pessev for his help in providing relevant near-IR filter passband information. We are grateful to the referee, James Rose, for his insightful comments that improved the content of this paper. THP gratefully acknowledges support in form of a Plaskett Fellowship at the Herzberg Institute of Astrophysics of the National Research Council of Canada. He also acknowledges support through an ESA Research Fellowship and partial financial support through grant GO-10129 from the Space Telescope Science Institute, which is operated by AURA, Inc., under NASA Contract NAS5-26555. This publication makes use of data products from the Two Micron All Sky Survey, which is a joint project of the University of

Massachusetts and the Infrared Processing and Analysis Center/California Institute of Technology, funded by the National Aeronautics and Space Administration and the National Science Foundation.

REFERENCES

Abraham, R. G., van den Bergh, S., Glazebrook, K., Ellis, R. S., Santiago, B. X., Surma, P., & Griffiths, R. E. 1996, ApJS, 107, 1
Anders, P., & Fritze-v. Alvensleben, U. 2003, A&A, 401, 1063
Balogh, M. L., Miller, C., Nichol, R., Zabludoff, A., & Goto, T. 2005, MNRAS, 360, 587
Barger, A. J., Aragon-Salamanca, A., Ellis, R. S., Couch, W. J., Smail, I., & Sharples, R. M. 1996, MNRAS, 279, 1
Bekki, K., & Couch, W. J. 2003, ApJ, 596, L13
Bekki, K., Couch, W. J., Shioya, Y., & Vazdekis, A. 2005, MNRAS, 359, 949
Belloni, P., Bruzual, A. G., Thimm, G. J., & Roser, H.-J. 1995, A&A, 297, 61
Benson, A. J., Ellis, R. S., & Menanteau, F. 2002, MNRAS, 336, 564
Bessell, M. S., & Brett, J. M. 1988, PASP, 100, 1134
Bertin, E., & Arnouts, S. 1996, A&AS, 117, 393
Bruzual, G., & Charlot, S. 2003, MNRAS, 344, 1000
Bothun, G. D. & Dressler, A. 1986, ApJ, 301, 57
Bundy, K., Ellis, R. S., & Conselice, C. J. 2005, ApJ, 625, 621
Byrd, G., & Valtonen, M. 1990, ApJ, 350, 89
Caldwell, N., & Rose, J. A. 1997, AJ, 113, 492
Caldwell, N., Rose, J. A., & Dendy, K. 1999, AJ, 117, 140
Caldwell, N., Rose, J. A., & Concannon, K. D. 2003, AJ, 125, 2891
Coleman, G. D., Wu, C.-C., & Weedman, D. W. 1980, ApJS, 43, 393
Conselice, C. J. 1997, PASP, 109, 1251
Conselice, C. J. 2003, ApJS, 147, 1
Couch, W. J. & Sharples, R. M. 1987, MNRAS, 229, 423
Cowie, L. L., Songaila, A., Hu, E. M., & Cohen, J. G. 1996, AJ, 112, 839
Daddi, E., Cimatti, A., & Renzini, A. 2000, A&A, 362, L45
Daddi, E., Cimatti, A., Renzini, A., Fontana, A., Mignoli, M., Pozzetti, L., Tozzi, P., & Zamorani, G. 2004, ApJ, 617, 746
Dressler, A. & Gunn, J. E. 1983, ApJ, 270, 7
Dressler, A., Smail, I., Poggianti, B. M., Butcher, H., Couch, W. J., Ellis, R. S., & Oemler, A. J. 1999, ApJS, 122, 51
Drory, N., Bender, R., Feulner, G., Hopp, U., Maraston, C., Snigula, J., & Hill, G. J. 2003, ApJ, 595, 698
Drory, N., Bender, R., Feulner, G., Hopp, U., Maraston, C., Snigula, J., & Hill, G. J. 2004, ApJ, 608, 742
Ferraro, F. R., Montegriffo, P., Origlia, L., & Fusi Pecci, F. 2000, AJ, 119, 1282
Franx, M. 1993, ApJ, 407, L5
Galaz, G. 2000, AJ, 119, 2118
Georgakakis, A., Hopkins, A. M., Afonso, J., Sullivan, M., Mobasher, B., & Cram, L. E. 2006, MNRAS, 367, 331
Giavalisco, M., et al. 2004, ApJ, 600, L93
Goto, T. 2004, A&A, 427, 125
Goudfrooij, P., Alonso, M. V., Maraston, C., & Minniti, D. 2001, MNRAS, 328, 237
Gunn, J. E., & Gott, J. R. I. 1972, ApJ, 176, 1
Hempel, M., & Kissler-Patig, M. 2004, A&A, 428, 459
Kauffmann, G. & Charlot, S. 1998, MNRAS, 294, 705
Kinney, A. L., Calzetti, D., Bohlin, R. C., McQuade, K., Storchi-Bergmann, T., & Schmitt, H. R. 1996, ApJ, 467, 38
Larson, R. B. 1975, MNRAS, 173, 671
Le Fèvre, O., et al. 2004, A&A, 428, 1043
Maraston, C. 1998, MNRAS, 300, 872
Maddox, S. J., Efstathiou, G., Sutherland, W. J., & Loveday, J. 1990, MNRAS, 243, 692
Michard, R. 2005, A&A, 441, 451
Miller, N. A., & Owen, F. N. 2001, ApJ, 554, L25
Mobasher, B., Ellis, R. S., & Sharples, R. M. 1986, MNRAS, 223, 11
Mobasher, B., et al. 2004, ApJ, 600, L167
Mobasher, B., et al. 2007, ApJS in press, astro-ph/0612344
Moore, B., Katz, N., Lake, G., Dressler, A., & Oemler, A. 1996, Nature, 379, 613
Moore, B., Lake, G., & Katz, N. 1998, ApJ, 495, 139
Mouhcine, M., & Lançon, A. 2003, A&A, 402, 425
Newberry, M. V., Boroson, T. A., & Kirshner, R. P. 1990, ApJ, 350, 585
Oke, J. B. 1974, ApJS, 27, 21
Pérez-González, P. G., Gil de Paz, A., Zamorano, J., Gallego, J., Alonso-Herrero, A., & Aragón-Salamanca, A. 2003a, MNRAS, 338, 508
Pérez-González, P. G., Gil de Paz, A., Zamorano, J., Gallego, J., Alonso-Herrero, A., & Aragón-Salamanca, A. 2003b, MNRAS, 338, 525
Persson, S. E., Aaronson, M., Cohen, J. G., Frogel, J. A., & Matthews, K. 1983, ApJ, 266, 105
Persson, S. E., Murphy, D. C., Krzeminski, W., Roth, M., & Rieke, M. J. 1998, AJ, 116, 2475
Poggianti, B. M., Smail, I., Dressler, A., Couch, W. J., Barger, A. J., Butcher, H., Ellis, R. S., & Oemler, A. J. 1999, ApJ, 518, 576
Poggianti, B. M., & Wu, H. 2000, ApJ, 529, 157
Poggianti, B. M., et al. 2001, ApJ, 563, 118
Poggianti, B. M., Bridges, T. J., Komiyama, Y., Yagi, M., Carter, D., Mobasher, B., Okamura, S., & Kashikawa, N. 2004, ApJ, 601, 197
Puzia, T. H., Zepf, S. E., Kissler-Patig, M., Hilker, M., Minniti, D., & Goudfrooij, P. 2002, A&A, 391, 453
Quintero, A. D., et al. 2004, ApJ, 602, 190
Ravindranath, S., et al. 2006, ArXiv Astrophysics e-prints, arXiv:astro-ph/0606696
Renzini, A. 1981, Ann. Phys., 6, 87
Rose, J. A., Gaba, A. E., Caldwell, N., & Chaboyer, B. 2001, AJ, 121, 793
Sánchez-Blázquez, P., Gorgas, J., Cardiel, N., & González, J. J. 2006, A&A, 457, 809
Schlegel, D. J., Finkbeiner, D. P., & Davis, M. 1998, ApJ, 500, 525
Shioya, Y., Bekki, K., Couch, W. J., & De Propris, R. 2002, ApJ, 565, 223
Shioya, Y., Bekki, K., & Couch, W. J. 2004, ApJ, 601, 654
Simpson, C., et al. 2006, MNRAS, 373, L21
Sirianni, M., et al. 2005, PASP, 117, 1049
Smail, I., Morrison, G., Gray, M. E., Owen, F. N., Ivison, R. J., Kneib, J.-P., & Ellis, R. S. 1999, ApJ, 525, 609
Smail, I., Kuntschner, H., Kodama, T., Smith, G. P., Packham, C., Fruchter, A. S., & Hook, R. N. 2001, MNRAS, 323, 839
Springel, V., et al. 2005, Nature, 435, 629
Tran, K. H., Franx, M., Illingworth, G., Kelson, D. D., & van Dokkum, P. 2003, ApJ, 599, 865
Tran, K. H., Franx, M., Illingworth, G. D., van Dokkum, P., Kelson, D. D., & Magee, D. 2004, ApJ, 609, 683
Zabludoff, A. I., Zaritsky, D., Lin, H., Tucker, D., Hashimoto, Y., Shectman, S. A., Oemler, A., & Kirshner, R. P. 1996, ApJ, 466, 104